Modeling of an impact system with a drift

Ekaterina Pavlovskaia and Marian Wiercigroch
Department of Engineering, King's College, Aberdeen University, Aberdeen, AB24 3UE, United Kingdom

Celso Grebogi
Instituto de Física, Universidade de São Paulo, Caixa Postal 66318, 05315-970 São Paulo, SP, Brazil
(Received 1 June 2001; published 25 October 2001)

A physical model to examine impact oscillators has been developed and analyzed. The model accounts for the viscoelastic impacts and is capable to mimic the dynamics of a bounded progressive motion (a drift), which is important in practical applications. The system moves forward in stick-slip phases, and its behavior may vary from periodic to chaotic motion. A nonlinear dynamic analysis reveals a complex behavior and that the largest drift is achieved when the responses switch from periodic to chaotic, after a cascade of subcritical bifurcations to period one. Based on this fact, a semianalytical solution is constructed to calculate the progression of the system for periodic regimes and to determine conditions when periodicity is lost.

DOI: 10.1103/PhysRevE.64.056224 PACS number(s): 05.45.−a

I. INTRODUCTION

The dynamics of physical systems, whose components make intermittent contacts with each other and whose contact points are progressively drifting, is of a considerable importance in practical applications. Imagine, for example, a vibroimpact system driving a pile into the ground. During its operation, the driving module moves downwards, and its motion may be viewed as a sum of a progression with constant velocity and bounded oscillations. The simplest physical model exhibiting such behavior is comprised of a mass loaded by a force having static and harmonic components, and a dry friction slider, as shown in Fig. 1(a). This model was introduced and preliminarily analyzed in [1,2]. Despite its simple structure, a very complex dynamics was revealed. The main result from that work was a finding that the best progression occurs when the system responds periodically. The dynamics of that system is similar to the dynamics of impact oscillators (see, for example, [3–11]).

A special feature of impacting systems that might prove to be useful in the current study is the instability caused by low-velocity collisions, so-called grazing effects. The first important work in this area was done by Nordmark [12], who studied analytically the occurrence of singularities in a piecewise linear system. This work has been further expanded by thorough investigations of two-dimensional maps, where some universal behavior has been found [13–16].

A wide range of impacting models have been applied to simulate and analyze engineering systems operating within bounded dynamic responses. For example, in heat-exchanger tubes [17], thin-wall milling [18], ultrasonic drilling of hard materials [19], and a vibroimpact ground moling system [20], impacting models have proved to be useful. However, as it has been mentioned earlier, very few [1,2] have considered systems with drift. To fill this gap, a detailed mathematical modeling and nonlinear dynamic analysis of a model is given in this paper. The model includes the viscoelastic properties of the contact between the impacting mass and the frictional slider, which were previously neglected.

II. MATHEMATICAL MODELING

We consider a simple two degree-of-freedom system, which is shown in Fig. 1(b). A mass m is driven by an external force containing a harmonic component of amplitude P_d, frequency Ω and phase shift φ, and a static component, P_s. The slider has weightless top and bottom plates connected to each other by a linear spring with stiffness k, and a viscous damper with damping coefficient c. Similarly to the stick-slip phenomena reported in [21,22], the progressive motion of the mass occurs when the force acting on the slider exceeds the threshold of the dry friction force P_f. X_m, X_t, X_b represent the absolute displacements of the mass, slider top, and slider bottom, respectively. It is assumed that the model operates in a horizontal plane, or gravity force is included in a static force.

We assume that at the initial moment $t=0$, there is a distance between the mass and the slider top called gap G. The gap G is one of the system parameters and it may be positive, negative, or equal to zero. If $G>0$, there is a transitional phase when the mass moves freely without any interaction with the slider; if $G=0$, the mass is touching the slider top, but the slider spring is not compressed; and finally, if $G<0$, there is a precompression of the slider.

As the system may operate in stick-slip phases, its dynamic dimension may vary. For the case when the mass and the slider move separately, the dynamics of the system is described by one second- and two first-order differential equations

$$m\ddot{X}_m = P_s + P_d \cos(\Omega t + \varphi),$$
$$c(\dot{X}_t - \dot{X}_b) + k(X_t - X_b) = 0, \quad (1)$$
$$\dot{X}_b = 0.$$

When the mass and the slider are in contact, their motion is described by one second-order and one first-order differential equations, which may be either oscillatory

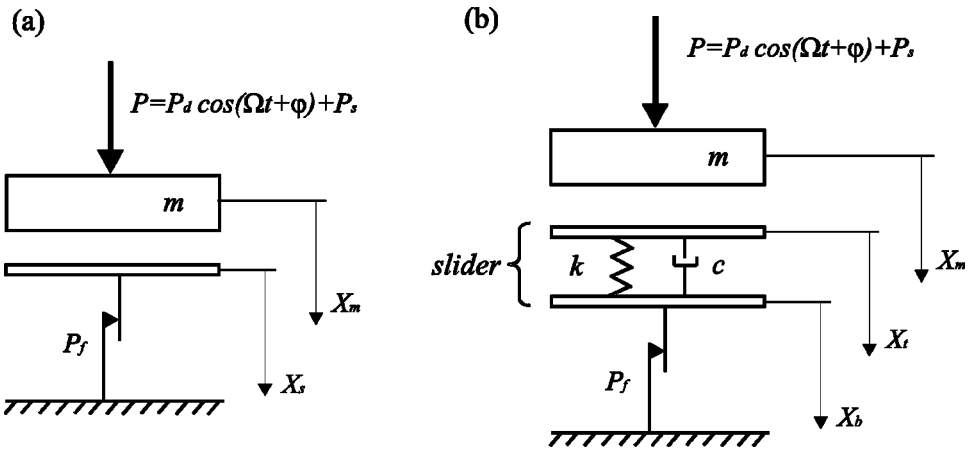

FIG. 1. Physical models of progressive impact systems; (a) previous model [1,2], (b) new model.

$$m\ddot{X}_m + c(\dot{X}_t - \dot{X}_b) + k(X_t - X_b) = P_s + P_d \cos(\Omega t + \varphi),$$
$$\dot{X}_b = 0, \tag{2}$$

or progressive

$$m\ddot{X}_m = -P_f + P_s + P_d \cos(\Omega t + \varphi),$$
$$c(\dot{X}_t - \dot{X}_b) + k(X_t - X_b) = P_f. \tag{3}$$

Note that for Eqs. (2) and (3), the displacement of the slider top X_t is in phase with the displacement of the mass X_m, but differs by a gap

$$X_t = X_m - G.$$

The equations of motion (1)–(3) are to be transformed to sets of first-order differential equations. These sets will use the following nondimensional variables:

$$\tau = \Omega_0 t, \quad x = \frac{k}{P_{max}} X_m, \quad y = \frac{dx}{d\tau} = \frac{k}{\Omega_0 P_{max}} \dot{X}_m,$$
$$z = \frac{k}{P_{max}} X_t, \quad v = \frac{k}{P_{max}} X_b,$$

and parameters

$$\omega = \frac{\Omega}{\Omega_0}, \quad \Omega_0 = \sqrt{\frac{k}{m}}, \quad a = \frac{P_d}{P_{max}}, \quad b = \frac{P_s}{P_{max}},$$
$$d = \frac{P_f}{P_{max}}, \quad \xi = \frac{c}{2m\Omega_0}, \quad g = \frac{k}{P_{max}} G,$$

where P_{max} is a normalization constant force.

As has been discussed above, the considered system may operate at the time in one of the following modes: (i) no contact; (ii) contact without the progression of the slider; (iii) contact with the progression of the slider; and for each, a careful consideration will be given next. For the simplicity of further analysis, the dimensionless friction threshold force d is set to 1.

A. No contact

If the displacement of the mass is smaller than the displacement of the slider top plus the gap,

$$x < z + g, \tag{4}$$

then the mass and the slider top move separately. The motion of the mass may be determined from the following set of equations:

$$x' = y,$$
$$y' = a \cos(\omega\tau + \varphi) + b, \tag{5}$$

where $'$ denotes $d/d\tau$. Equations of motion for the top and the bottom of the slider are

$$z' = -\frac{1}{2\xi}(z - v), \tag{6}$$

$$v' = 0. \tag{7}$$

B. Contact without progression

This mode occurs when the relative displacement of the mass exceeds the displacement of the slider top, i.e.,

$$x \geq z + g, \tag{8}$$

and the force acting on the mass from the slider is greater than zero but smaller than the threshold of the dry friction force, which may be expressed as

$$0 < 2\xi z' + (z - v) < 1. \tag{9}$$

In this case, the mass and the slider top move together but without progression, and the second equation of Eq. (5) has additional elastic and viscous terms

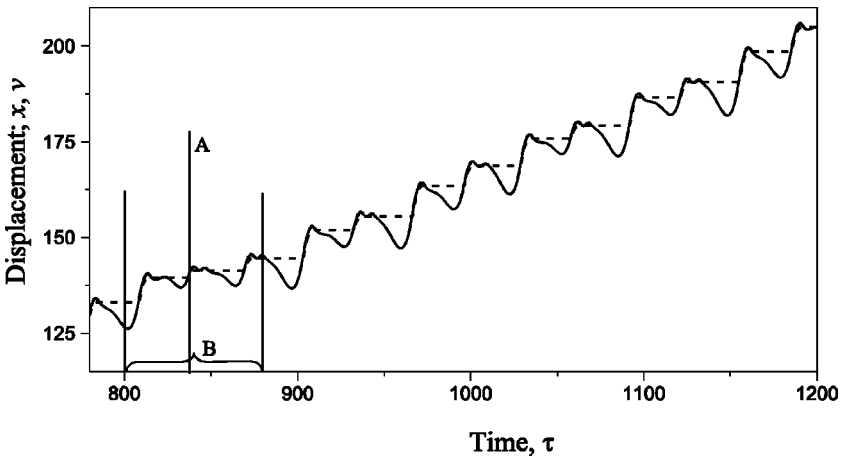

FIG. 2. Displacement of the mass, x (solid curve) and slider bottom, v (dash curve) versus time, τ calculated for $a=0.3$, $b=0.22$, $\omega=0.2$, $g=0.02$, $\varphi=\pi/2$, and $\xi=0.01$. The zoom-up windows of regions A and B are presented in Figs. 3(a) and 3(b), respectively.

$$x'=y,$$
$$y'=-2\xi z'-(z-v)+a\cos(\omega\tau+\varphi)+b. \tag{10}$$

The velocity of the slider top is equal to the velocity of the mass, and the displacement of the slider top is in phase with the mass displacement but differs by g in position

$$z'=x', \tag{11}$$

$$x=z+g. \tag{12}$$

When there is no progression, the bottom of the slider remains stationary, hence, its velocity is equal to zero

$$v'=0. \tag{13}$$

C. Contact with progression

When the displacement of the mass is equal to or greater than the displacement of the slider top plus the gap [see Eq. (8)], and the force acting on the mass is greater than the threshold of dry friction force

$$2\xi z'+(z-v)\geqslant 1, \tag{14}$$

then the mass and the top and the bottom of the slider are moving together, and the progression takes place. Equations of motion for mass are

$$x'=y,$$
$$y'=a\cos(\omega\tau+\varphi)+b-1. \tag{15}$$

The displacement and the velocity of the slider top are described as before [see Eqs. (11) and (12)]. The velocity of the slider bottom motion may be calculated from the expression below

$$v'=z'+\frac{1}{2\xi}(z-v-1). \tag{16}$$

Having spelled out different distinct phases of motion, let us now define a set of auxiliary functions, P_1, P_2, P_3, and P_4, which will be used to obtain the final form of the equations of motion. We will use the Heaviside function $H(\cdot)$ to describe the piecewise linear nature of the system.

$$P_1=P_1(x,z)=H(x-z-g), \tag{17}$$
$$P_2=P_2(z,z',v)=H(2\xi z'+z-v),$$
$$P_3=P_3(z,z',v)=H(2\xi z'+z-v-1),$$
$$P_4=P_4(v')=H(v').$$

Finally, the equations of motion for the system being considered may be given by the following set of first-order differential equations:

$$x'=y,$$
$$y'=a\cos(\omega\tau+\varphi)+b-P_1P_2(1-P_3)(2\xi y+z-v)-P_1P_3, \tag{18}$$
$$z'=P_1y-(1-P_1)(z-v)/2\xi,$$
$$v'=P_1P_3P_4[y+(z-v-1)/2\xi].$$

Equations (18) will be used to conduct nonlinear dynamic analysis (Sec. III) by a means of numerical integration, and also to construct an algorithm to determine periodic responses (Sec. IV).

III. NONLINEAR DYNAMIC ANALYSIS

The basic function of the investigated system is to overcome the frictional force and move downwards. Despite the fact that the considered model has only two degrees of freedom, the dynamics of this system is very complex, varying from different types of periodic to chaotic types of motion. A typical steady-state time history is presented in Fig. 2, where the absolute displacement of the impacting mass (solid line) and the bottom of the slider (dash line) are shown. As the responses of the slider top and the mass are indistinguishable in Fig. 2, a zoom up of the time history between 839.7 and 841 (window A) is depicted in Fig. 3(a). The vertical distance between the solid and dash lines, for any time when the mass is in contact with the slider top, is equal to the gap g.

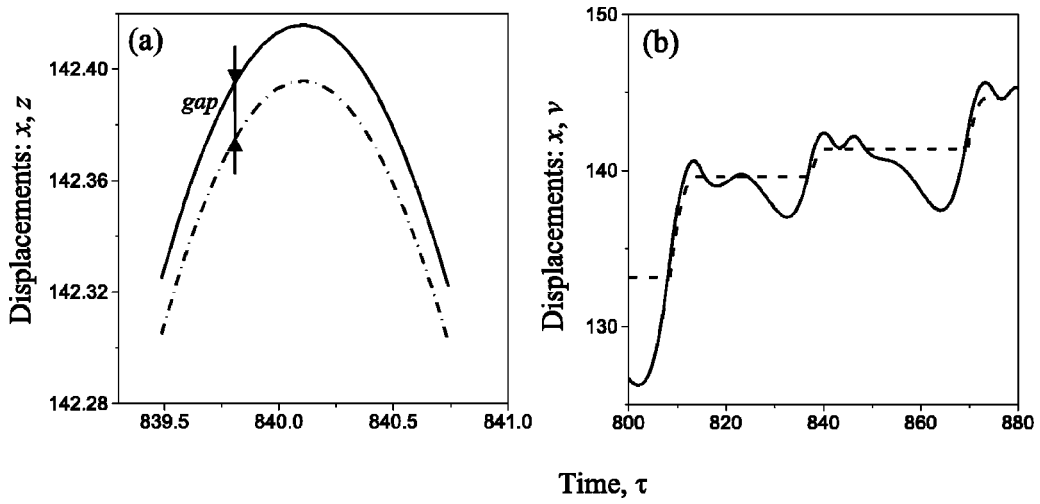

FIG. 3. (a) Displacement of the mass, x (solid curve) and slider top, z (dash and dotted curve) versus time, τ for $a=0.3$, $b=0.22$, $\omega=0.2$, $g=0.02$, $\varphi=\pi/2$, and $\xi=0.01$; (b) Displacement of the mass, x (solid curve) and slider bottom, v (dash curve) versus time, τ for the same values of parameters.

The progressive motion of the slider bottom and the mass may be seen from Fig. 3(b). The phases when the mass and the slider are in contact and out of contact are essential for the dynamics of this system and they are discussed in detail later in the paper, where the periodic solution is constructed.

Our study has revealed that the largest drift (the best progression) is achieved for period-one motion [Fig. 4, curve (d)], which may be clearly seen by examining displacement of the slider bottom (dash lines) in Fig. 4. The steady-state responses at $\tau\in(800,1200)$ for the same system parameters are depicted on Figs. 5(a)–5(e). Figure 5 shows an important sequence of subcritical bifurcations, where the system bifurcates from period four [Fig. 5(b)] to period two [Fig. 5(c)], then from period two to period one [Fig. 5(d)]. A transition from period-one to chaotic motion with a high-frequency component [Fig. 5(e)] determines the interval of static force b for which the best progression exists. In addition, the system may exhibit chaotic motion at large [Fig. 5(a)], and this will be discussed later. The periodic motion depicted in Fig. 5(f) is similar to the one obtained for a four-dimensional rotor system studied by Heijden [23]. The high-frequency oscillations are caused by the mass being in permanent contact with the slider.

Further in this section, a brief overview of the global system dynamics will be given by a means of bifurcation diagrams, Poincaré maps, and Lyapunov exponents, which have been computed using *Dynamics* software [24].

Since the displacements of the system elements (mass, top, and bottom of the slider) are moving from the origin, the mass velocity has been used to view the structural changes in the system responses due to the fact that it is bounded. Therefore, the bifurcation diagrams presented in Fig. 6 with the branching parameters as the static force and frequency of excitation, are constructed for the change of the mass velocity.

In Fig. 6(a), a bifurcation diagram for variable static force b is presented. The bifurcation structure is rather complex [13,16] and not typical of a smooth system because the vector field given by Eqs. (18) is nondifferentiable. As can be seen, the system responds chaotically for $b\in(0.0,0.1)$ with a narrow window of periodic motion, for $b\in(b_1,b_2)$. Then we have a large window of periodic motion for b in the

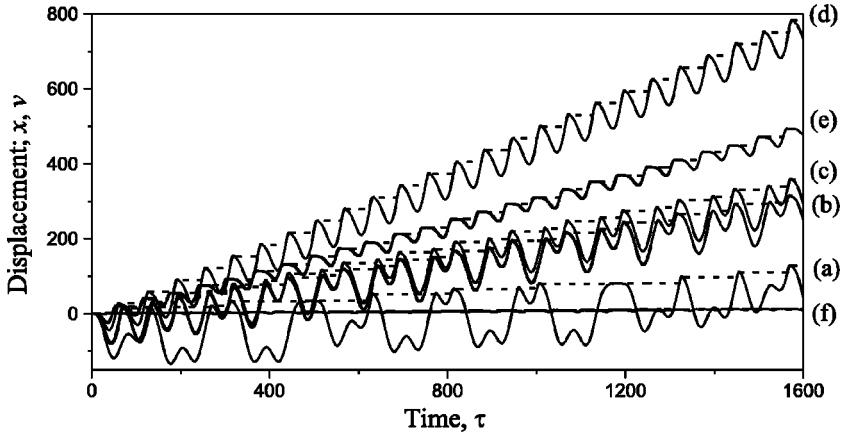

FIG. 4. Displacement of the mass, x (solid curves) and slider bottom, v (dash curves) versus time, τ calculated for $a=0.3$, $\omega=0.1$, $\xi=0.05$, $g=0.02$, $\varphi=\pi/2$, and (a) $b=0.05$; (b) $b=0.095$; (c) $b=0.1$; (d) $b=0.15$; (e) $b=0.19$, and (f) $b=0.27$.

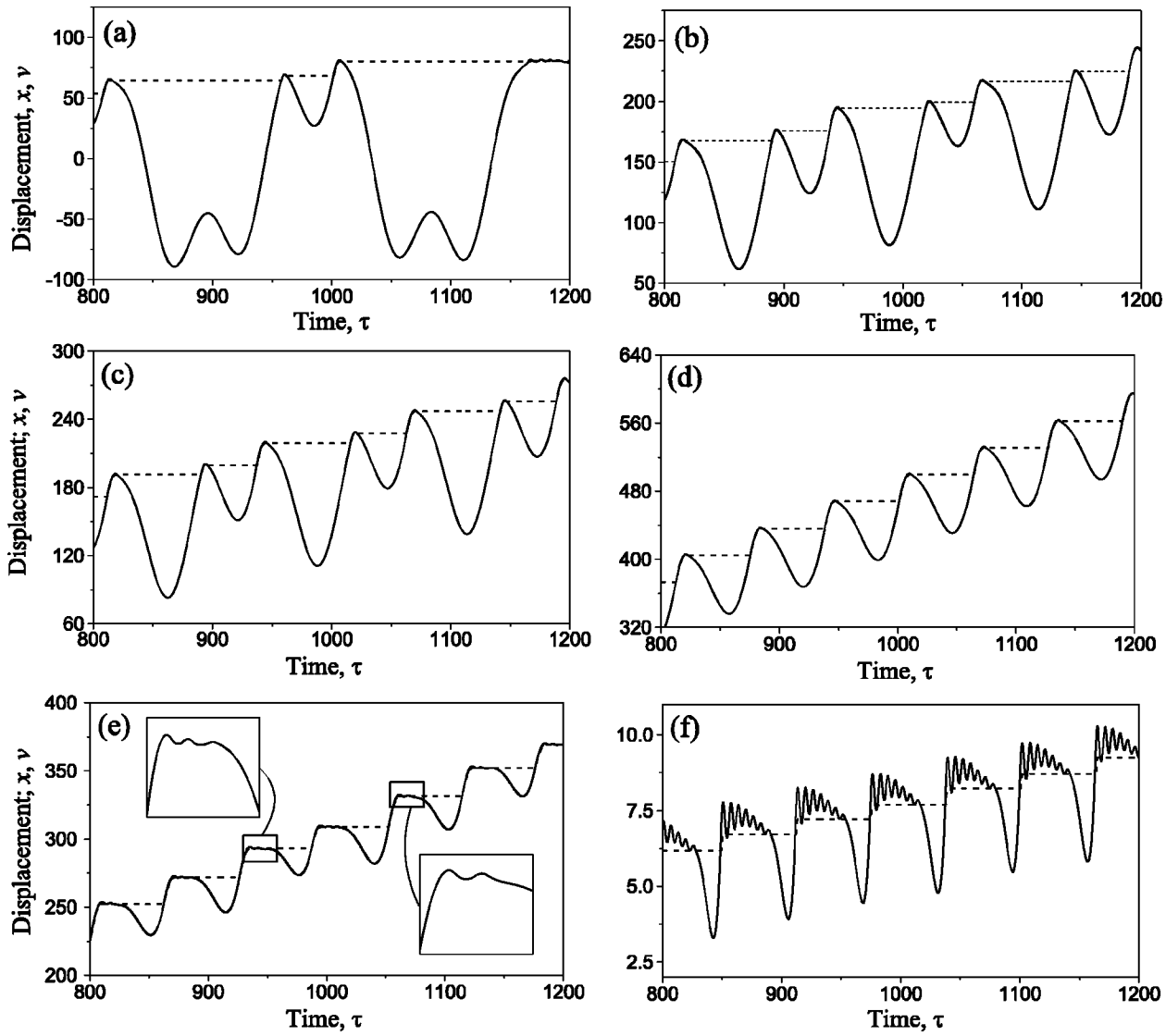

FIG. 5. Steady-state responses of the mass, x (solid curves) and slider bottom, v (dash curves) for $a=0.3$, $\omega=0.1$, $\xi=0.05$, $g=0.02$, $\varphi=\pi/2$, and (a) $b=0.05$; (b) $b=0.095$; (c) $b=0.1$; (d) $b=0.15$; (e) $b=0.19$, and (f) $b=0.27$.

interval (0.10,0.165), where its end is marked by a vertical dash line. Thereafter, a series of quasiperiodic and periodic windows appear. This branching parameter proved to be very useful for determining the regions of the best progression.

Figure 6(b) uses the frequency of excitation, ω as a branching parameter. The system starts up with a narrow chaotic window around $\omega=0.03$, and then oscillates periodically up to $\omega\approx0.25$, where a first period of doubling bifurcation occurs. The second period of doubling appears around $\omega=0.37$, leading eventually to chaos for ω in the interval (0.4,0.55). Then, the system has a window of periodic motion, initially with period two, which at $\omega\approx0.62$ doubles and at $\omega\approx0.68$ doubles again leading to chaotic motion starting approximately at $\omega\approx0.7$.

The observation of the bifurcation diagrams has brought some practical insight regarding the progression rates achieved by the system. By looking at the bifurcation diagram in Fig. 6(a), the end of the large periodic window is marked at $b\approx0.165$. Since the system equilibrium is moving towards larger displacements, one way to monitor the progression rate is to calculate progression in a finite time. In our experiments, we set up time τ equal to 50 periods of external loading. As can be clearly seen from Fig. 7, the maximum penetration rate coincides with the end of periodical regime, which occurs for $b\approx0.165$. Also, it is worth noting a few local maxima for higher values of b, which were mentioned by Krivtsov and Wiercigroch [1]. The information regarding the position of the maximum penetration rate (the end of periodic regime) has been used to develop a semianalytical algorithm for determining this point, and this will be outlined in the next section.

Apart from the velocity, the other bounded characteristic of the system is the difference between displacement of the mass and displacement of the slider bottom. This difference was used for construction of Poincaré maps. Poincaré maps for two different values of the frequency ω and fixed static

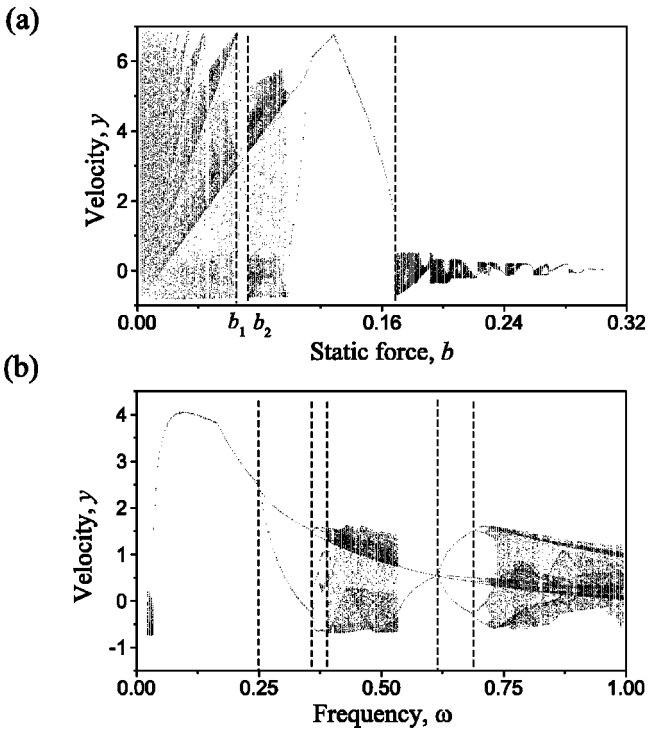

FIG. 6. Bifurcation diagrams (dash lines indicate borders of different regimes); (a) $y=f(b)$ for $a=0.3$, $\xi=0.05$, $\omega=0.1$, $g=0.02$, $\varphi=\pi/2$; (b) $y=f(\omega)$ for $a=0.3$, $b=0.15$, $\xi=0.05$, $g=0.02$, $\varphi=\pi/2$. Bifurcation diagrams are constructed as follows. The initial value of the branching parameter b (or ω) is set to the leftmost value 0.0 (0.02) in the (a) and (b). For this set of parameters, in order to exclude the transient behavior, the map is iterated 100 times without plotting anything. The next 300 iterations of the map produces 300 values of the velocity, y, which are plotted in the figure. Then a small increment is added to the branching parameter [in these figures it is equal to $(b(\text{or }\omega)_{max}-b(\text{or }\omega)_{min})/480$] and the procedure is repeated until the branching parameter reaches the rightmost value. The repetition of the procedure by decreasing the branching parameter from rightmost to leftmost value showed no hysteresis in the system.

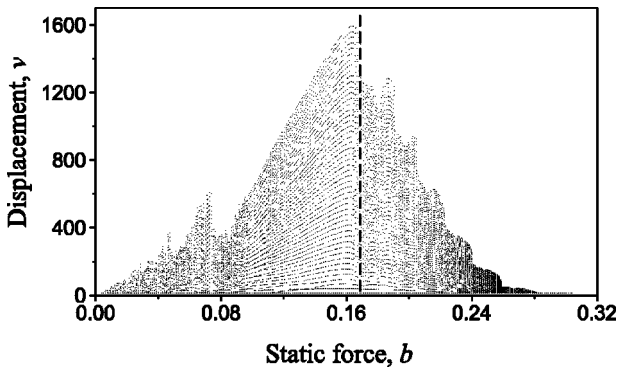

FIG. 7. Progressions for $a=0.3$, $\xi=0.05$, $\omega=0.1$, $g=0.02$, $\varphi=\pi/2$. Dash line indicates the value of static force corresponding to the maximum progression.

and dynamic forces and damping coefficient are given in Fig. 8. They demonstrate a strange attractor development, which appears to be similar to the one reported in [5]. As can be seen, the higher the frequency, the more complex the behavior of the system.

IV. PERIODIC BEHAVIOR

The numerical analysis of the system shows that the period-one motion presented in Fig. 5(d) is the most efficient from the progression point of view. Since our system is piecewise linear, this periodic solution may be constructed by matching linear solutions at points of discontinuities (e.g., [25]).

The following approach has been adopted here. Initially, it is assumed that the displacement and velocity of the mass have certain (yet unknown) values. Starting from these values, the system operates in one of the phases described in Sec. II. The solutions for each phase are constructed. The final displacements and velocities of the preceding phase define the initial conditions for the next one. This enables us also to calculate the time interval for which a particular phase persists. Finally, the initial conditions of the first phase are being found from the periodicity condition. The current paper refrains from a detailed account of the method used to determine the periodic solution as this will be given in a separate publication. However, a skeleton of the method will be discussed below.

In Fig. 9, a sequence of four phases for the one period of period-one motion is presented. This typical pattern is comprised of the following:

Phase I – progression: the mass and the slider are in contact.

Phase II – contact without progression: the mass and the slider are in contact but the slider bottom is not moving.

Phase III – no contact: the mass and the slider are moving separately.

Phase IV – contact without progression: the same as Phase II.

In order to simplify our consideration, the beginning of progression was chosen as an initial point. In this moment, the mass and the slider top are moving together, and the force acting on the mass from the slider reaches the threshold value. Taking into account that the velocities of the mass and the slider top are equal, and their displacements differ by the gap, the following relation between the initial displacement and velocity may be written:

$$2\xi y_0+(x_0-g-v_0)=1. \tag{19}$$

As the initial displacement of the slider bottom, v_0 does not influence the mass motion, it is set to zero. Thus, we have

$$x_0=1+g-2\xi y_0. \tag{20}$$

The other unknown is the time at this initial moment τ_0. This means that we need to evaluate a phase shift between the external force and the system response at the beginning of the process

$$\psi_0=\varphi+\omega\tau_0. \tag{21}$$

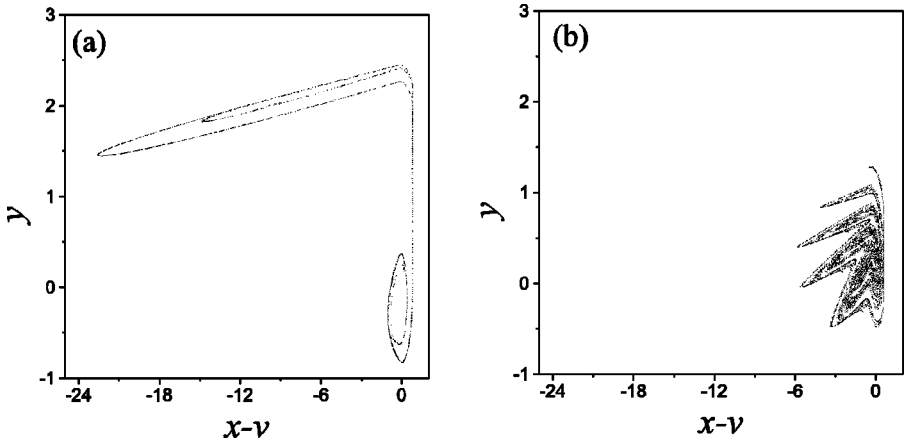

FIG. 8. Poincaré sections for $a=0.3$, $b=0.1$, $\xi=0.01$, $g=0.02$, $\varphi=\pi/2$; (a) $\omega=0.25$, (b) $\omega=1.4$.

There are two periodic conditions for the mass displacement and velocity

$$x(\tau+T)=x(\tau)+\Delta,$$
$$y(\tau+T)=y(\tau), \tag{22}$$

where T is the period and Δ is progression of the slider per period. We will look for the periodic regimes, where the period T is equal to the period of external loading

$$T=\frac{2\pi}{\omega}. \tag{23}$$

Thus, three unknown functions ψ_0, x_0, and y_0 may be found from Eqs. (22) and (23). However, the arbitrary solution of these equations cannot guarantee that x_0 and y_0 satisfy Eq. (20). For this reason, we first substitute x_0 by the function of y_0 [expression (20)], and then construct a special function F to monitor a difference between the exact periodic solution and the one calculated for these arbitrary initial conditions

$$F=\sqrt{[x(\tau+T)-x(\tau)-\Delta]^2+[y(\tau+T)-y(\tau)]^2}. \tag{24}$$

If the minimum of this function is equal to zero, then the periodic regime exists, and the durations of all four phases may be determined. To provide a reader with more details about how the solution is constructed, Phase I is carefully considered in the Appendix.

The constructed semianalytical solution gives a means to investigate the dependence of the progression per period as a function of the system parameters. Figure 10 shows the influence of the static force b on the progression per period for different values of dynamic force a under fixed damping coefficient ξ and frequency of external loading ω. As may be seen from the graphs, the progression reaches the maximum values at some certain values of static force and close to this maximum the periodic solution breaks down (dash line). The existence of this maximum is in a good agreement with the numerical calculations, known experimental data [26], and the previous analytical models [1,2].

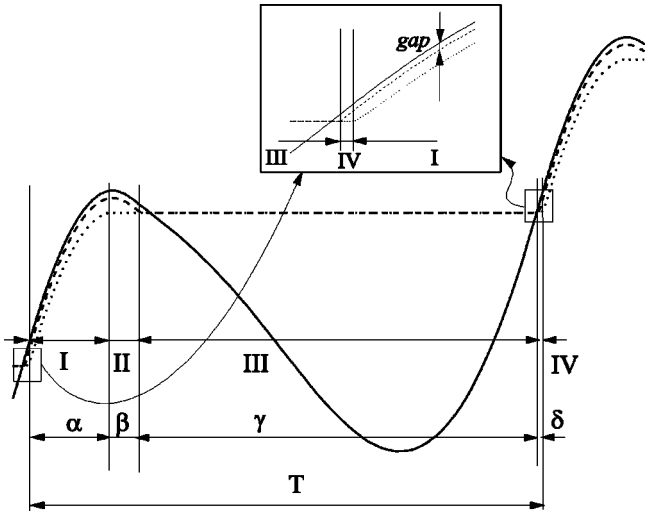

FIG. 9. Four phases of a periodic response; solid line – displacement of the mass, dash line – displacement of the slider top, dotted line – displacement of the slider bottom. The blow-up window shows the displacements of the mass, slider top, and bottom at the beginning and at the end of the period.

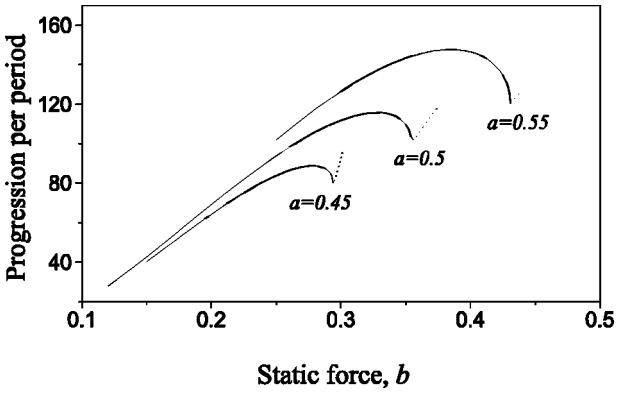

FIG. 10. Influence of static force on progression for $\xi=0.01$, $\omega=0.1$, $g=0.02$, $\varphi=\pi/2$ calculated using the developed semianalytical method.

V. CLOSING REMARKS

In this paper, a model of an impact system with a dry frictional slider was developed and analyzed. The system operates with bounded progressive responses (a drift). The system parameters were chosen to experience stick-slip phenomenon, which is used to mimic dynamics of engineering systems (e.g., downhole drilling or ground moling). The model has been mathematically formulated and the equations of motion developed. A typical nonlinear dynamic analysis has revealed a complex behavior ranging from periodic to chaotic motion. The bifurcation diagrams were constructed using variation of the mass velocity as the displacement has a drift. It was found that the maximum progression coincides with the end of periodic regime and the beginning of chaotic motion (the largest Lyapunov exponent jumps from -10^{-6} to 10^{-3}). This information was used to construct a semianalytical solution, which is useful to determine the conditions for the best progression rates. It is hoped that this model, having important practical applications, will be useful for other physical applications (e.g., motion of suspended particles in fluid) and will stimulate further work on the dynamics of systems with drifts.

ACKNOWLEDGMENTS

E.P. and M.W. would like to acknowledge the financial support from EPSRC under Grant No. GR/N16341. C.G. was supported by FAPESP and CNPq. The authors would like to thank Steve Bishop (UCL), Tomasz Kapitaniak (TU-Lodz), Frantisek Peterka (Czech Academy of Science), and Yutaka Yoshitake (University of Nagasaki), for valuable and constructive comments on the manuscript.

APPENDIX

In order to demonstrate the idea of construction of periodic solution, let us consider in detail the first phase (progression) of the period depicted in Fig. 9. The framework for the remaining phases is similar. The adopted method allows us to find step-by-step durations of all phases as functions of initial values x_0, y_0, and ψ_0. Then by satisfying the periodicity condition as it is explained in Sec. IV, these values and progression per period may be found.

We start our consideration from the progression phase in the moment, when this phase has just begun [x_0 and y_0 are connected by relation Eq. (20)]. Using the initial values of x_0, y_0, and ψ_0, we may construct the solution of Eq. (15) as

$$x(\tau)=-\frac{a}{\omega^2}[\cos(\omega\tau+\psi_0)-\cos(\psi_0)]+\frac{1}{2}(b-1)\tau^2+y_0\tau - \frac{a}{\omega}\tau\ \sin(\psi_0)+x_0, \tag{A1}$$

$$y(\tau)=\frac{a}{\omega}[\sin(\omega\tau+\psi_0)-\sin(\psi_0)]+(b-1)\tau+y_0. \tag{A2}$$

Having obtained $x(\tau)$ and taking into account that $z(\tau)=x(\tau)-g$, the displacement of the slider bottom may be found by solving of Eq. (16)

$$v(\tau)=x(\tau)-g-1+2\xi y_0\exp\left(-\frac{\tau}{2\xi}\right). \tag{A3}$$

When the progression condition, Eq. (14) fails, another phase, contact without progression, begins, and thus, the end of the first phase may be found from the following equation:

$$y(\alpha)-y_0\exp\left(-\frac{\alpha}{2\xi}\right)=0. \tag{A4}$$

By substituting Eq. (A2) for Eq. (A4), we obtain

$$\frac{a}{\omega}[\sin(\omega\alpha+\psi_0)-\sin(\psi_0)]+(b-1)\alpha+y_0-y_0\exp\left(-\frac{\alpha}{2\xi}\right)=0. \tag{A5}$$

The above equation enables us to calculate the length of the first phase α as a function of the initial conditions y_0 and ψ_0

$$\alpha=\alpha(y_0,\psi_0). \tag{A6}$$

Then, the progression of the slider per period Δ may be expressed with respect to α as

$$\Delta=v(\alpha)=x(\alpha)-g-1+2\xi y_0\exp\left(-\frac{\alpha}{2\xi}\right). \tag{A7}$$

At this point, the progression phase has finished and another phase, contact without progression, has begun. Therefore, the initial conditions for the second phase are calculated using expressions (A1) and (A2)

$$x_{\mathrm{I}}=x(\alpha),\quad y_{\mathrm{I}}=y(\alpha). \tag{A8}$$

The process should be continued by solving the equations of motion for the next phase with the initial conditions x_i, y_i and phase shift $\psi_i=\psi_{i-1}+\varepsilon\omega$, where $i=$I,II,III,IV and $\varepsilon=\alpha,\beta,\gamma,\delta$. Finally, x_0 and y_0 may be found from the periodicity conditions

$$x_{\mathrm{IV}}=x(\delta)=\Delta+x_0,\qquad y_{\mathrm{IV}}=y(\delta)=y_0. \tag{A9}$$

[1] A.M. Krivtsov and M. Wiercigroch, Meccanica **34**, 425 (1999).
[2] A.M. Krivtsov and M. Wiercigroch, Chaos, Solitons Fractals **11**, 2479 (2000).
[3] A.E. Kobrinskii, *Dynamics of Mechanisms with Elastic Connections and Impact Systems* (ILIFFE Books Ltd, London, 1969).
[4] S.W. Shaw and P.J. Holmes, J. Sound Vib. **90**, 129 (1983).
[5] J.M.T. Thompson and R. Ghaffari, Phys. Rev. A **27**, 1741 (1983).
[6] S. Foale and S.R. Bishop, Philos. Trans. R. Soc. London, Ser. A **338**, 547 (1992).
[7] F. Peterka, Acta Tech. CSAV **4**, 462 (1974); **5**, 569 (1974); F. Peterka and J. Vacik, *ibid.* **2**, 161 (1981); T. Kotera and F. Peterka, *ibid.* **6**, 747 (1981); **1**, 92 (1982); **3**, 255 (1984).
[8] M. Wiercigroch and V.T.W. Sin, ASME J. Appl. Mech. **65**(3), 657 (1998).
[9] S. Natsiavas, J. Sound Vib. **134**(2), 315 (1989).
[10] B. Blazejczyk-Okolewska and T. Kapitaniak, Chaos, Solitons Fractals **7**, 1455 (1996).
[11] C. Budd and F. Dux, Philos. Trans. R. Soc. London, Ser. A **347**, 365 (1994).
[12] A.B. Nordmark, J. Sound Vib. **145**, 279 (1991).
[13] W. Chin, E. Ott, H.E. Nusse, and C. Grebogi, Phys. Rev. E **50**, 4427 (1994).
[14] W. Chin, E. Ott, H.E. Nusse, and C. Grebogi, Phys. Lett. A **201**, 197 (1995).
[15] F. Casas, W. Chin, C. Grebogi, and E. Ott, Phys. Rev. E **53**, 134 (1996).
[16] S. Banerjee and C. Grebogi, Phys. Rev. E **59**, 4052 (1999).
[17] H. Goyda and C. Teh, J. Pressure Vessel Technol. **111**, 394 (1989).
[18] M. Davies and B. Balachandran, Nonlinear Dyn. **22**, 375 (2000).
[19] M. Wiercigroch, R.D. Neilson, and M.A. Player, Phys. Lett. A **259**, 91 (1999).
[20] K.-C. Woo, A.A. Rodger, R.D. Neilson, and M. Wiercigroch, Chaos, Solitons Fractals **11**, 2515 (2000).
[21] M. Wiercigroch, J. Sound Vib. **175**, 700 (1994).
[22] U. Galvanetto and S.R. Bishop, Int. J. Mech. Sci. **36**, 683 (1994).
[23] G.H.M. van der Heijden, Dyn. Stab. Syst. **15**, 159 (2000).
[24] J.A. Yorke and H.E. Nusse, *Dynamics* (Springer-Verlag, New York, 1998).
[25] S.J. Hogan, Chaos, Solitons Fractals **11**, 495 (2000).
[26] M. Wiercigroch, A. Krivtsov, and J. Wojewoda, in *Nonlinear Dynamics and Chaos of Mechanical Systems with Discontinuities*, edited by M. Wiercigroch and A. de Kraker (World Scientific, Singapore, 2000), Chap. 16.